Built-In Self Test of CMOS-MEMS Accelerometers*

N. Deb and *R. D. (Shawn) Blanton*
Center for Silicon System Implementation
Department of Electrical and Computer Engineering
Carnegie Mellon University
Pittsburgh, PA 15213
email: {ndeb, blanton}@ece.cmu.edu

Abstract

A built-in self-test technique for MEMS that is applicable to symmetrical microstructures is described. A combination of existing layout features and additional circuitry is used to make measurements from symmetrically-located points. In addition to the normal sense output, self-test outputs are used to detect the presence of layout asymmetry that are caused by local, hard-to-detect defects. Simulation results for an accelerometer reveal that our self-test approach is able to distinguish misbehavior resulting from local defects and manufacturing process variations.

1 Introduction

MicroElectroMechanical Systems (MEMS) are complex heterogeneous systems consisting of devices whose operation is based on the interactions of multiple energy domains. Commercial manufacture of MEMS has increased the need for cost-effective test methods that screen defective devices from good ones. With MEMS becoming increasingly complex and finding use in life-critical applications such as air-bags [1], bio-sensors [2], and aerospace applications [3], there is a growing need for robust fault models and test methods.

Of the currently used MEMS process technologies, surface micromachining is a popular one due to its well-developed infrastructure for depositing, patterning and etching of thin films for silicon integrated circuits. Surface micromachining enables the fabrication of high-quality MEMS devices because it is based on thin-film technology that combines control and flexibility in the fabrication process. Example applications of this technology include the digital micromirror display [4] and the accelerometer [5, 6]. Our work in MEMS test has therefore been focussed on surface micromachined devices. However, we believe our self-test approach can be easily applied to other process technologies.

MEMS manufacturing test is the process of identifying good devices in a batch of fabricated devices. The normal assumption is that the design is correct and that test is the process of verifying that the fabricated device is equivalent to the design. However, a device that passes traditional, specification-based manufacturing test may fail later during in-field operation. For example, a mechanical beam of an accelerometer may become stuck to the die surface due to a phenomenon known as stiction [7]. A stuck beam may mimic behavior similar to a device affected by an expected level of under-etch[1] [8]. By adjusting the electronics, either accelerometer can be easily calibrated to meet its operational specification. The danger, however, is that an accelerometer with a stuck beam may release in the field (*i.e.* defect healing) causing the accelerometer to go out of calibration, which then can possibly lead to failure. Detection or prevention of field failures can be accomplished through built-in self test (BIST).

As MEMS become more complicated and find a wider range of applications, the need for on-chip self-test features will grow. BIST for the manufacturing test of MEMS is yet to be common practice. However, progress in this area has been recently made [9, 10, 11, 12]. The work in [9] describes the self-test of a pressure sensor. In their approach, thermal actuation of the sensor's diaphragm is performed by driving current through a resistive heater. The heat generated increases the temperature of the air in the sensor's cavity creating a pressure that displaces the diaphragm. Using a similar technique, the authors of [11] use resistive heaters to increase the temperature of a MEMS infrared-imager array. Many commercial accelerometers use a self-test technique similar to the one described in [10]. In this approach, dedi-

*This research, sponsored by the National Science Foundation under grant MIP-9702678, has a patent pending.

[1]MEMS require a "release" processing step where sacrificial material is removed to free the microstructure. The release typically requires an etching step, and in the case where the etch varies, a device can be larger or smaller than desired.

0-7803-7542-4/02 $17.00 © 2002 IEEE

cated mechanical beams are used to generate an electrostatic force that mimics an external acceleration. It is useful for determining if the accelerometer's mechanical microstructure is free to move. Unlike our BIST approach however, this technique cannot be used until the electrostatic force is calibrated after manufacturing test. Finally, an idea for accelerometer self-test that exploits design symmetry is suggested in [12]. They propose to actuate the accelerometer one side at a time and then compare the two outputs obtained to detect any anomaly.

The MEMS device used in our analysis represents the most common sensor structure; the standard spring-beam, electrostatic comb-drive, single-axis, micromechanical accelerometer [5]. Commercially-manufactured devices such as accelerometers are usually affected by multiple failure sources. Failure sources for MEMS include but are not limited to foreign particles, etch variations, and stiction [13], each of which can lead to a variety of defects. For example, in [14] it is shown that particles can lead to defects that include broken and bridged structures with corresponding behaviors that range between benign and catastrophic. Many of these failure sources exhibit very similar misbehaviors and are difficult to distinguish from each other. This paper describes a BIST approach that samples outputs from symmetrically-located nodes of the MEMS microstructure. Increasing observability in this way allows one to identify misbehavior resulting from local defects as opposed to more benign causes, a problem not addressed by other self-test methods. Our BIST approach builds upon the fully differential sensing technique described in [15] and applies to a broad class of sensors and actuators that includes resonators [16], accelerometers, and gyroscopes [17]. Here, we have focussed on CMOS-MEMS [15] since the availability of multiple routing layers makes BIST in CMOS-MEMS more viable than in technologies where routability is limited.

2 Accelerometer Test

In previous work [8], we have shown that changes in device behavior due to global manufacturing variations (such as over/under-etch) may mimic those caused by point defects (such as particles). In such cases of misbehavior overlap, distinguishing between various failure sources becomes difficult. Among failure sources exhibiting similar misbehavior, the potential long-term effects of some are expected to be more harmful than others. Since misbehavior overlap hampers defect diagnosis, it also prevents more harmful defects from being distinguished from those which are benign. The BIST approach proposed here aims to resolve this issue through differential actuation and sensing. Our method uses existing device features to create two signals that should be identical in the nominal design but are unequal when asymmetry exists. If successful, the BIST will allow one to distinguish between harmful defects that cause asymmetries as opposed to those that preserve layout symmetry [2].

2.1 Normal Operation

We apply our self-test approach to a CMOS-MEMS [15] accelerometer. A simplified view of an accelerometer's mechanical microstructure is shown in Figure 1. For the purposes of clarity, we have omitted details of the serpentine spring structure, the multi-layered device structure, routed interconnects.

A MEMS accelerometer is a transducer that converts translational acceleration to an electrical signal that is typically a voltage. An accelerometer's mechanical component (*i.e.*, the sensor) can be viewed as a collection of primitive microstructures that include beams, anchors and a plate called the shuttle. Anchors attach beams to the die surface only at the positions shown in Figure 1. Anchored beams connected to the shuttle act as springs since they create a restoring force when the shuttle moves as a result of an acceleration. The remaining beams are typically referred to as "fingers". Accelerometer fingers are partitioned into two classes: fixed and movable. Fixed fingers are anchored to the die surface and therefore are not free to move. Movable fingers are attached to the shuttle and therefore can move along with the shuttle. Subsets of fixed and movable fingers also serve various purposes. The *sense* fingers enable measurement of shuttle movement in the X direction while *actuation* fingers are used to create an electrostatic force that moves the shuttle for testing purposes. *Dummy* fingers are not involved in the normal operation of the accelerometer but are used to enhance the manufacturability of the device.

An accelerometer's sensor behaves as a linear second-order system similar to a spring-mass-damper system. As already mentioned, the beams attached to the top and bottom of the shuttle act as restoring springs. The shuttle is capable of motion by virtue of the flexibility provided by these so-called spring beams. Motion at or near the anchor points is negligible so locations farthest away from the anchors experience the greatest amount of movement. Damping of the accelerometer is generated by the air surrounding it.

In response to an input acceleration, the shuttle moves from its resting position until the restoring force of the spring beams balances the inertial force caused by the acceleration. Each triplet of fixed-movable-fixed fingers constitutes a pair of capacitors, C_1 and C_2, as shown in Figure 1. At rest, the two capacitors are equal. Shuttle movement however causes the value of one capacitor to increase and the other to decrease. Shuttle movement is detected or

[2] Structural deformations that preserve layout symmetry are usually caused by normal process variations. Since these changes are permanent, it is safe to compensate for these deformations through electronic calibration.

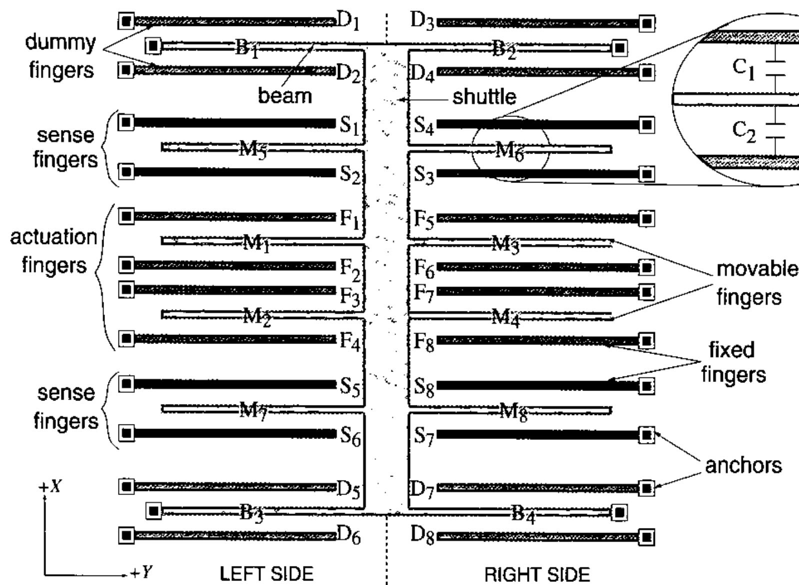

Applied voltage	Normal operation	Self-test operation
V_{act}	-	F_1, F_3, F_5, F_7
V_{nom}	$F_1 - F_8$ $M_1 - M_4$ $D_1 - D_8$ $B_1 - B_4$	F_2, F_4, F_6, F_8 $M_1 - M_4$ $D_5 - D_8$
V_{mp}	S_1, S_3, S_5, S_7	S_1, S_4, S_5, S_8 D_1, D_3
V_{mn}	S_2, S_4, S_6, S_8	S_2, S_3, S_6, S_7 D_2, D_4

Figure 2: Microstructure voltage biasing for normal and self-test operations.

Figure 1: Simplified top view of an accelerometer's mechanical microstructure.

"sensed" by electronics that detects change in the capacitances. With modulation voltage signals (*e.g.*, high frequency pulse train) of opposite phases applied to the fixed fingers, the finger triplet is a potential divider with the voltage output of the movable finger serving as the output sense signal. In the fully-differential sensing scheme [15], one phase of the modulation voltage (V_{mp}) is applied to the finger pairs $[S_1, S_3]$ and $[S_5, S_7]$ and the other phase (V_{mn}) is applied to $[S_2, S_4]$ and $[S_6, S_8]$ (see Figure 4(a) and Figure 2). A sense signal from electrically-connected sense fingers on the left (M_5 and M_7) and right (M_6 and M_8) sides are connected to inputs A_1 and A_2 of a differential amplifier (Figure 3), respectively, where the primary sense outputs $V_{sp} = V_{s_1} - V_{s_2}$ and $V_{sn} = V_{s_2} - V_{s_1}$ are produced. The fully-differential scheme of sensing has the advantage of rejecting any noise that is common to the left and right sides of the sensor.

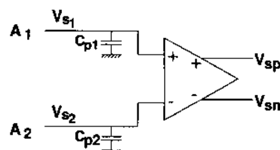

Figure 3: Schematic of a differential amplifier.

An electrostatic attraction force can be created to displace the shuttle for testing [10]. The voltage of the movable fingers for a shuttle at rest is called the *nominal* voltage (V_{nom}), and is simply the average of the modulation signal, namely $\frac{1}{T}\int_0^T V_{mp}dt$. Electrostatic actuation in the positive X direction is achieved by applying the actuation signals (V_{act}), usually DC or low frequency, to fingers $[F_1, F_3, F_5, F_7]$ and the nominal voltage to the fingers $[F_2, F_4, F_6, F_8]$, $[M_1 - M_4]$, and $[D_1 - D_8]$ (see Figure 1).

2.2 Self-Test Operation

Currently, self-test of commercial accelerometers is limited. BIST techniques used in industry [10] are focussed on input stimulus generation. In accelerometers produced by Analog Devices, Motorola and others, the accelerometer's shuttle is moved to its maximum position using actuation fingers so that the full-scale sense output is generated. The inability to generate a full-scale output, within some tolerance limits, means the accelerometer has failed self test. Using this form of BIST for manufacturing test is difficult since the amount of actuation voltage needed can only be determined after the part has been tested and calibrated. It is also ineffective for distinguishing misbehavior stemming from different sources. For example, a BIST output that is larger (smaller) than expected can be either caused by over-etch (under-etch) or broken (stuck) beams. Hence, its ability to identify hard-to-detect defects (*e.g.*, asymmetry due to local defects) is limited.

In the BIST technique proposed in [12], the accelerometer's shuttle is moved twice, once using the right actuation fingers and again using the left actuation fingers. Failure results when the two resulting sense outputs do not match, presumably, within some tolerance level. Unlike the techniques currently used in industry, this method does not necessarily require calibration before it can be used. However,

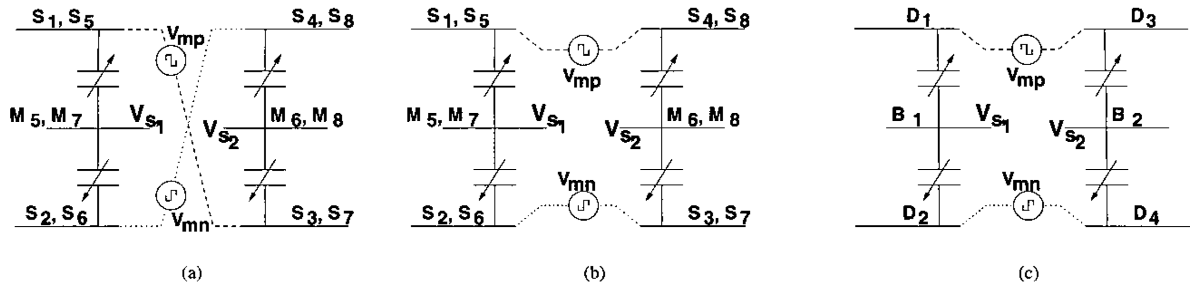

Figure 4: Schematics showing the modulation schemes for (a) fully differential normal operation, (b) differential BIST operation using normal sense fingers, (c) differential BIST operation using spring beams.

its ability to identify hard-to-detect defects is limited since all test observations are made from the normal sense output. Moreover, it is difficult to implement on chip since sample-and-hold circuitry is required to store the first measurement.

The differential BIST approach proposed in this paper aims to detect hard-to-detect defects that occur during manufacture or operation in the field. Its differential nature implies that it is independent of any calibration and therefore its also suitable for manufacturing test. If successful, the BIST will allow one to distinguish between defects that lead to asymmetries as opposed to those more benign deformations that preserve layout symmetry. Therefore, our approach is primarily targeted at defects escapes.

Our self-test technique is focussed on observation and therefore complements existing and proposed approaches that focus on stimulus generation [10, 12]. It creates and compares signals from pairs of symmetrically-located points on the accelerometer's micromechanical structure. Specifically, these sense points include the normal sense fingers and the spring beams that are surrounded by dummy fingers. Dummy fingers are manufacturing-enhancing structures located near the spring beams (see Figure 1). They are used to ensure that the spring beams have etch-loading properties similar to those experienced by the movable and fixed fingers. During self-test, the dummy fingers have additional modulation signals applied and the spring beams are used as additional sensing signals. A differential amplifier is used to detect any difference between symmetrically-located fingers and beams. Obviously, the signal nodes that are compared must all be electrically isolated from each other, a feature that is easily achieved using the multiple routing layers available in a CMOS process. For each sense-point pair, a separate differential amplifier is used. Additional amplifiers for self-test increases cost in terms of area overhead but has the advantage of reduced parasitic capacitance and interference.

Local defects that introduce undesirable asymmetry between the left and right sides will cause the two symmetrically located sense outputs, V_{s_1} and V_{s_2}, to be unequal. If the difference $|V_{s_1} - V_{s_2}| > T$, where T is some pre-determined threshold, then asymmetry is detected. The polarity of the difference signal $V_{s_1} - V_{s_2}$ also grossly localizes the defect site. For example, a contamination that creates a high-resistve bridge between fingers F_1 and M_1 will hinder the motion of the sensor's left side more than that of the right side. Hence, the right sense output V_{s_1} (from $[M_5,M_7]$) will be less than V_{s_2} (from $[M_6,M_8]$) causing $V_{s_1} - V_{s_2}$ will be negative. In the opposite case, $V_{s_1} - V_{s_2}$ will be positive.

The operational details of the self-test scheme are now explained. To move the shuttle in the positive X direction, the nominal voltage is applied to fingers $[F_2, F_4, F_6, F_8]$, $[M_1 - M_4]$, and $[D_5, D_8]$ and actuation voltages are applied to fingers $[F_1, F_3, F_5, F_7]$ (see Figure 1 and Figure 2). The sense signal is sampled from different pairs of points:

- Sensing from the regular sense fingers for self-test purposes can be easily achieved by the scheme illustrated in Figure 4(b). Modulation signals of one phase (V_{mp}) are applied to the finger pairs $[S_1, S_4]$ and $[S_5, S_8]$ while those of the other phase (V_{mn}) are applied to the finger pairs $[S_2, S_3]$ and $[S_6, S_7]$. Note that this scheme is derived from the nominal one shown in Figure 4(a) by interchanging the phases of the modulation signals on the right side. Sense signals from finger pairs $[M_5, M_7]$ and $[M_6, M_8]$ are directed to the inputs A_1 and A_2, respectively, of a dedicated differential amplifier like the one shown in Figure 3.
- For sensing from the spring beams, opposite phases of modulation signals are applied to dummy finger pairs $[D_1, D_3]$ and $[D_2, D_4]$ (see Figure 4(c)). The sense signals from spring beams B_1 and B_2 are directed to the inputs A_1 and A_2, respectively, of another dedicated differential amplifier.

Self-test using movement in the negative X direction can be achieved in a similar fashion.

The multi-conductor nature of CMOS-MEMS allows extensive routing and electrical isolation of fingers that are

mechanically connected to the same shuttle, characteristics that make implementation of this BIST approach practicable. For example, in CMOS-MEMS, the sense voltage outputs from the spring beams can be electrically isolated very easily. This type of electrical isolation is much harder to achieve in other processes such as MUMPS [23] because of its single conducting layer.

The accelerometer is susceptible to both global and local manufacturing variations. Since the prime objective of our BIST technique is to detect left-right asymmetry, it is clear that global variations will affect both sides equally and therefore V_{s_1} and V_{s_2} will be affected equally, implying V_{s_1}/V_{s_2} will, in theory, be unaffected. But local manufacturing variations (such as local over/under etch, curvature variations, *etc.*) that lead to left-right asymmetry will result in unequal actuation forces on the left and right sides which in turn will lead to unequal sense outputs. Hence, this self-test approach is sensitive to local variations while being immune to global variations. For this reason, the difference $|V_{s_1} - V_{s_2}|$ or the ratio V_{s_1}/V_{s_2} is more significant than the absolute values of V_{s_1} and V_{s_2}.

Ideally, the self-test mechanism itself must not falsely indicate device failure. So the self-test actuation scheme should prevent the sense signal from being corrupted by the actuation signal even in the presence of left-right asymmetry caused by local manufacturing variations. The differential nature of our scheme guarantees that the actuation signal (*i.e.*, voltage) of each polarity is equally applied to both the left and right sides. In short, one polarity is applied to the fingers $[F_1, F_7]$ and the other to $[F_3, F_5]$. If, for example, the inter-finger capacitors on the right side are smaller than those on the left side, the resulting currents will therefore be unequal (less on the right side). The differential nature of our approach guarantees that current due to the actuation signal of each polarity has contributions from both the left (higher capacitance) and right (lower capacitance) sides. Therefore, the total current of each polarity is the same. Hence, given first-order manufacturing variations, the currents of the two polarities cancel and do not contribute to the differential self-test sense signal.

3 Simulation Results

A CMOS-MEMS accelerometer with the parameters listed in Table 1 is modified to include the necessary characteristics to implement our BIST approach. Specifically, switches are used to interchange the polarity of modulation signals applied to finger pairs $[S_3, S_7]$ and $[S_4, S_8]$, to control the application of modulation signals to the dummy fingers $[D_1 - D_4]$, and to select one of the two self-test difference signals if only one output pin is reserved for self-test. Simulation experiments are performed to examine the capability of this approach to detect asymmetry caused by:

Parameter	Value	Unit
Resonant frequency (f_x)	12.5	kHz
Sensor sensitivity	0.88	mV/G
Modulation voltage amplitude	5.0	V
Actuation voltage amplitude	1.5	V
Input referred noise	100	$\mu G/\sqrt{Hz}$
Bandwidth of baseband sense signal	500	Hz

Table 1: Nominal values for design and measured parameters of an accelerometer design used for simulation.

1. A single dielectric particle acting as a bridge between a pair of structures where at least one is movable;
2. A variation in vertical misalignment between fixed and movable fingers caused by curl mismatch [21];
3. A variation in local etch [22];
4. Unequal parasitics in the interconnects from the self-test sense points to the differential sense amplifier.

The targeted defects is guided by our interaction with industry as well as our own experience. For example, particles can originate from the clean room but also from the removal of the sacrificial layer during the release step. Particles formed out of the sacrificial layer can be as large as a few μm and are therefore large enough to act as bridges between structures.

Simulation experiments were conducted using NODAS [22], an AHDL (Analog Hardware Descriptive Language) simulator for mixed-domain circuits. NODAS has been shown to closely match experimental results [22]. The efficacy of NODAS as a reliable and much faster simulator than finite element analysis has also been demonstrated [18]. Both the electro-mechanical microstructure and electronic circuitry are simulated together. The electronic circuitry is based on a design [19] that has been fabricated and validated with CMOS-MEMS devices.

One of the parameters used to decide pass/fail for an accelerometer is its resonant frequency (f_x) for translation in the X direction. The acceptable range for resonant frequency includes a maximum deviation of $\pm 25\%$ from the nominal value, which translates to a range of $9.4kHz - 15.6kHz$ for the accelerometer design of Table 1. The acceptable range for the normal sense signal is $\pm 20\%$ from the nominal value ($10.5mV$), which implies a range of $8.4mV - 12.6mV$. If the bandwidth of the processed sense signal is restricted to about $500Hz$ then a reasonably low noise voltage floor of about $2\mu V$ can be achieved.

Defect location (%)	f_x (kHz)	Normal sense output (mv)	Self-test finger outputs				Self-test beam outputs			
			V_l^f (mV)	V_r^f (mV)	$V_l^f - V_r^f$ (μV)	$1-\frac{V_l^f}{V_r^f}$ (%)	V_l^b (mV)	V_r^b (mV)	$V_l^b - V_r^b$ (μV)	$1-\frac{V_l^b}{V_r^b}$ (%)
None	12.53	10.52	5.256	5.259	-3	0	1.851	1.853	-2	0
10	13.12	9.58	4.785	4.788	-3	0	1.643	1.670	-27	1.6
20	14.00	8.40	4.195	4.197	-2	0	1.338	1.411	-73	5.2
30	15.32	6.98	3.490	3.492	-2	0	1.016	1.149	-133	11.5

Table 2: Test outputs for a single bridge defect located at different points between spring beam B_1 and dummy finger D_1 of Figure 1.

Defect location (%)	f_x (kHz)	Normal sense output (mv)	Self-test finger outputs				Self-test beam outputs			
			V_l^f (mV)	V_r^f (mV)	$V_l^f - V_r^f$ (μV)	$1-\frac{V_l^f}{V_r^f}$ (%)	V_l^b (mV)	V_r^b (mV)	$V_l^b - V_r^b$ (μV)	$1-\frac{V_l^b}{V_r^b}$ (%)
None	12.53	10.52	5.256	5.259	-3	0	1.851	1.853	-2	0
0	13.74	8.30	4.544	3.761	783	20.8	1.539	1.541	-2	0
10	14.09	7.85	4.347	3.499	848	24.2	1.465	1.466	-1	0
20	14.57	7.27	4.089	3.183	906	28.5	1.370	1.371	-1	0

Table 3: Test outputs for a single bridge defect located at different points bet ween movable finger M_6 and fixed finger S_3 of Figure 1.

In the application our BIST approach to the accelerometer, self-test outputs are created from normal sense fingers and spring beams. Depending on the particular nature of an asymmetry, one output may be more suited than the other at observing the effects of a defect. Also, the asymmetries detected at one output need not be a subset of those detected at the other. Hence, the use of self-test outputs from both beams and fingers, and possibly other sites, is necessary to minimize defect escapes.

In the following subsections, the symbols V_l^b and V_r^b will be used to refer to the self-test outputs sampled from the spring beams B_1 and B_2 (see Figure 1), respectively. Similarly, V_l^f and V_r^f will represent self-test outputs sampled from the regular sense finger pairs $[M_5, M_7]$ and $[M_6, M_8]$ (see Figure 1), respectively. The voltage difference between each pair of self-test signals must be more than the $2\mu V$ noise floor to be considered significant.

3.1 Beam Bridges

A bridge defect can be caused by particulate matter that attaches a movable beam to an adjacent structure (*e.g*, a dummy finger) thereby hindering its motion. Due to the four-fold symmetry of the accelerometer, simulation of a bridge defect has been limited to one quadrant of the layout. Specifically, beam B_1 of the upper left quadrant of Figure 1 is used. Column 1 of Table 2 indicates the defect location expressed as a percentage of beam length. The 0% point is the anchored end of the beam and the 100% point is where the beam meets the shuttle. Columns 2 and 3 list the values of resonant frequency and normal sense output, respectively, for bridge defects located at different locations along the beam.

As the defect location moves from the anchor end of the beam to the end where it is attached to the shuttle, the beam stiffness increases. Consequently, shuttle displacement decreases. Also the layout asymmetry becomes more pronounced resulting in an increased difference between the two beam sense outputs V_l^b and V_r^b.

The listed resonant frequency values shown in Table 2 are all within the acceptable range, indicating these defects will pass a resonant frequency test. The normal sense output is outside its acceptable range only for the 30% point. Hence, in a majority of cases, a test based on resonant frequency and normal sense output will be ineffective. The finger sense outputs V_l^f and V_r^f hardly diverge because of the stiffness of the shuttle which means virtually equal displacements on both sides. However, the beam self-test outputs V_l^b and V_r^b do indicate the presence of an asymmetry.

3.2 Finger Bridges

A finger bridge defect is similar to a beam bridge defect except that it is located between a movable finger and a fixed finger. Naturally, it acts as a hindrance to shuttle motion. In this analysis the material of the bridging defect has been assumed to be dielectric since such defects are harder to detect. As before, the symmetry of the accelerometer is used

δH_{right}	f_x	Normal sense output	Self-test finger outputs				Self-test beam outputs			
			V_l^f	V_r^f	$V_l^f - V_r^f$	$1 - \frac{V_l^f}{V_r^f}$	V_l^b	V_r^b	$V_l^b - V_r^b$	$1 - \frac{V_l^b}{V_r^b}$
(μm)	(kHz)	(mv)	(mV)	(mV)	(μV)	(%)	(mV)	(mV)	(μV)	(%)
0	12.53	10.52	5.256	5.259	-3	0	1.851	1.853	-2	0
+0.5	12.51	10.44	5.248	5.193	55	-1.0	1.841	1.836	5	-0.3
+1.0	12.51	10.23	5.224	5.001	223	-4.4	1.810	1.789	21	-1.2
+1.5	12.51	9.87	5.177	4.695	482	-10.2	1.760	1.712	48	-2.8
+2.0	12.51	9.42	5.115	4.309	806	-18.7	1.696	1.616	80	-4.9

Table 4: Test outputs for variations in height mismatch between all fixed and movable fingers on the right side of the sensor.

Etch variation	f_x	Normal sense output	Self-test finger outputs				Self-test beam outputs			
			V_l^f	V_r^f	$V_l^f - V_r^f$	$1 - \frac{V_l^f}{V_r^f}$	V_l^b	V_r^b	$V_l^b - V_r^b$	$1 - \frac{V_l^b}{V_r^b}$
(μm)	(kHz)	(mv)	(mV)	(mV)	(μV)	(%)	(mV)	(mV)	(μV)	(%)
+0.025	12.33	10.30	5.404	4.897	507	-10.3	1.837	1.789	48	-2.7
+0.020	12.37	10.34	5.375	4.967	408	-8.2	1.840	1.801	39	-2.2
+0.010	12.45	10.43	5.315	5.110	205	-4.0	1.845	1.826	19	-1.0
0	12.53	10.52	5.256	5.259	-3	0	1.851	1.853	-2	0
-0.010	12.61	10.61	5.197	5.414	-217	4.0	1.858	1.881	-23	1.2
-0.020	12.69	10.71	5.136	5.574	-438	7.9	1.865	1.910	-45	2.3
-0.025	12.73	10.76	5.105	5.656	-551	9.7	1.869	1.925	-56	2.9

Table 5: Test outputs for etch variations between the left and right sides of the sensor.

to limit simulations to the upper right quadrant of the layout. An inter-finger defect that bridges fingers M_6 and S_3 in the upper right quadrant of Figure 1 is considered. An inter-finger bridge defect is modeled using the approach in [18]. Defect location is expressed as a percentage of movable finger length. The 0% point is the movable finger tip, and the 100% point is the movable finger base where it meets the shuttle.

The results in Table 3 indicate that a finger bridge defect may pass a resonant frequency test but will fail a sensitivity test. However, the normal sense output by itself does not indicate an asymmetry. The beam self-test outputs V_l^b and V_r^b hardly diverge and hence are ineffective. However, the finger self-test outputs V_l^f and V_r^f diverge significantly and clearly indicate the presence of asymmetry.

3.3 Finger Height Mismatch

Ideally, the fingers should all be at the same height above the die surface. But variations in parameters such as temperature and residual stress lead to finger height mismatch. Height mismatch between the fixed and movable fingers reduces inter-finger overlap and hence inter-finger capacitance. Here it is shown how left-right asymmetry caused by such height mismatch can be detected by this BIST approach. Without loss of generality, the finger height mismatch is assumed to exist on the right side of the accelerometer only ($\delta H_{left} = 0$). Table 4 lists the simulation results. Column 1 lists the relative height mismatch which is expressed as $\delta H_{right} - \delta H_{left} = \delta H_{right}$. Results for negative values of mismatch have not been separately simulated since they would yield similar results. Such symmetrical behavior is exhibited by CMOS-MEMS since the gap between the substrate and the accelerometer fingers is $20\mu m$.

With increasing height mismatch, the difference in sensing between the two sides increases, as evident from both $[V_l^b, V_r^b]$ and $[V_l^f, V_r^f]$. The resonant frequency remains virtually unchanged clearly indicating a resonant frequency test will not detect this form of asymmetry. The normal sense output reveals an acceptable reduced voltage due to the reduced sense capacitance. Hence, a test based on resonant frequency and normal sense output will be ineffective in detecting the asymmetry. However, the difference between the finger self-test outputs V_l^f and V_r^f clearly indicate the presence of asymmetry. Although not as sensitive, the beam self-test outputs V_l^b and V_r^b also vary with the amount of mismatch and therefore indicate an asymmetry as well.

3.4 Local Etch Variations

An etching process is used in fabrication to remove sacrificial material in order to free the micromechanical sensor. Material removal through an etching process varies with time and space even though such variation is not desirable. For example, a rectangular structure designed to have length

Parasitic mismatch (%)	f_x (kHz)	Normal sense output (mv)	Self-test finger outputs				Self-test beam outputs			
			V_l^f (mV)	V_r^f (mV)	$V_l^f - V_r^f$ (μV)	$1-\frac{V_l^f}{V_r^f}$ (%)	V_l^b (mV)	V_r^b (mV)	$V_l^b - V_r^b$ (μV)	$1-\frac{V_l^b}{V_r^b}$ (%)
0	12.53	10.52	5.256	5.259	-3	0	1.851	1.853	-2	0
1.25	12.51	10.50	5.239	5.265	-26	0.5	1.843	1.850	-7	0.4
2.5	12.51	10.49	5.221	5.270	-49	0.9	1.836	1.847	-11	0.6
3.75	12.51	10.48	5.203	5.274	-71	1.3	1.828	1.845	-17	0.9
5.0	12.51	10.47	5.186	5.280	-94	1.8	1.819	1.841	-22	1.2

Table 6: Test outputs for variations in the parasitic interconnect capacitance of the differential amplifier.

l and width w may be subjected to more than the intended etch by a length δ, resulting in dimensions $[l-2\delta, w-2\delta]$. This is due to the fact that each side-wall of the rectangular structure shifts inwards by δ so that each dimension reduces by 2δ. This type of etch variation is called over-etch. In a similar fashion, under-etch causes an oversize structure of size $[l+2\delta, w+2\delta]$.

Etch variation can also be local in nature. Consider two rectangular structures that are designed to be identical but during fabrication they are subjected to different etch variations, δ_1 and δ_2. As a result, the two structures will have different dimensions, causing a left-right asymmetry.

Without loss of generality, we assumed in simulation that the accelerometer's left side has nominal etch while the right side has ether over- or under-etch. Table 5 gives the simulation results. Column 1 lists the relative etch mismatch. The mismatch in etch variation is positive when the right side is more etched than the left side.

As the relative over-etch increases, the sensitivity of the right side reduces because of the loss in the inter-finger capacitance. Consequently, the differences $|V_l^f - V_r^f|$ and $|V_l^b - V_r^b|$ increase. For increasing levels of relative under-etch, two counteracting effects become significant. The increased beam thickness on the right side causes increased stiffness which in turn reduces displacement. However, the reduced inter-finger gap causes higher inter-finger capacitance which more than offsets the loss of sensitivity. In any case, a higher level of local etch variation leads to a greater difference between each pair of self-test outputs.

A test based on resonant frequency test and normal sense output will not detect the presence of this type of asymmetry because both parameters are within their respective acceptable ranges. The finger self-test outputs V_l^f and V_r^f diverge and hence indicate an asymmetry. The beam self-test outputs V_l^b and V_r^b indicate an asymmetry as well. As in the case of finger height mismatch, $|V_l^f - V_r^f| \sim 10 \times |V_l^b - V_r^b|$, which means the finger self-test outputs are stronger indicators of this type of asymmetry as compared to the beam self-test outputs.

3.5 Parasitic Variation

Ideally, the sensing circuitry for self-test should only be sensitive to asymmetries in the micromechanical sensor and not the external electronics (including interconnects). In reality, a difference signal may be due to variation external to the sensor area, such as in the interconnects which carry the self-test sense signals to the inputs of the differential amplifier. With reference to the differential amplifier in Figure 3, assume the interconnect capacitances (C_{p1} and C_{p2}) are unequal. The objective is to determine the extent to which the parasitic capacitance mismatch due to such interconnect asymmetry will produce a significant sense amplifier output. The maximum value of the parasitic mismatch can be used to decide a suitable threshold for detection of sensor asymmetry during self-test. The nominal interconnect capacitance is assumed to be $40fF$. A maximum mismatch of 5% between the two interconnects is considered, assuming that a good layout design and a stable process can restrict such variations to the presumed limit. Without loss of generality, we assumed that the interconnect from the left sense points (for both the finger and beam outputs) are larger than the right. The simulation results are listed in Table 6.

The parasitic mismatch has a more pronounced effect for the beam self-test outputs $[V_l^b, V_r^b]$ as compared to the finger self-test outputs $[V_l^f, V_r^f]$ since the beam self-test signals are much weaker. It is observed that $|V_l^f - V_r^f|$ is less sensitive to variations in the interconnect when compared to variation in local etch and finger height. However, the same is not true for the beam self-test outputs.

Interconnect capacitance mismatch does indeed cause self-test outputs to exceed the noise floor. However, in a majority of the cases considered, the output magnitude does not rival that produced by the other defects. This implies that variations of up to 5% in the interconnect capacitance are unlikely to falsely indicate asymmetry in the micromechanical structure of the accelerometer. Only a beam bridge defect that is located close to its anchor point will produce a beam self-test output difference that is not significantly larger than that produced by interconnect mismatch.

4 BIST Implementation

Since simulation alone is not sufficient for validating the differential BIST approach, we have designed a prototype by adding a subset of the BIST features to the accelerometer design of [19]. The chip has been fabricated and the added self-test capabiities are currently being characterized. The BIST implementation was limited to finger self-test for the purpose of validation. The layout of the prototype design is shown in Figure 5. The technology used is a three-metal-one-poly, $0.6 \mu m$ CMOS process.

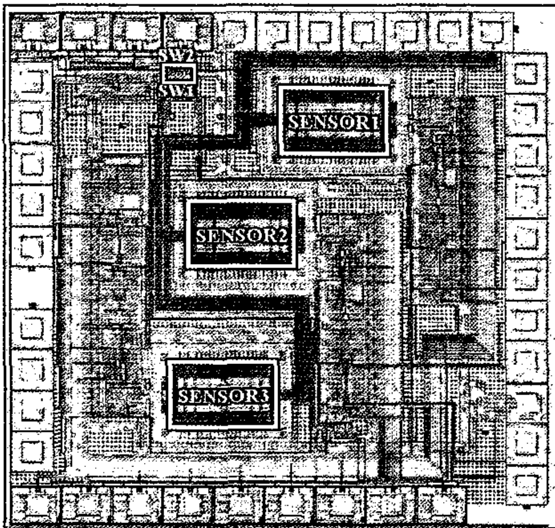

Figure 5: Layout of the BIST design showing the location of the sensors and the switch-based BIST control circuitry.

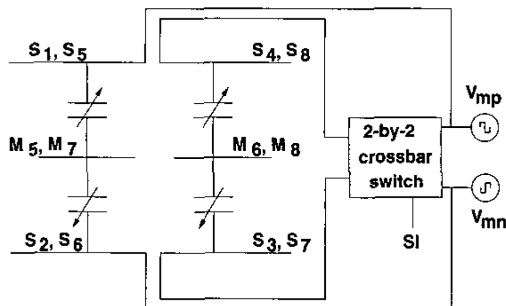

Figure 6: Schematic showing control circuitry required for BIST operation.

The control circuitry for BIST is illustrated in Figure 6. The two phases of the modulation voltage signal are V_{mp} and V_{mn}. The digital self-test input pin (SI) is driven to a logic zero during normal operation. For SI=0, the capacitive network reduces to the one shown in Figure 4(a). Self-test is activated when SI=1. For this case, the capacitive network reduces to the one shown in Figure 4(b).

The overhead of the BIST circuit includes routing area for two extra wires for the modulation signals and area for simple 2-by-2 cross-bar switch. The area of the switch is $105 \mu m \times 35 \mu m$, which is $< 0.06\%$ of the of the total die area ($2.5mm \times 2.5mm$). The routing for the two extra modulation lines in the sensor was achieved by using the POLY1 layer. An extra input pin is required for activating the self-test. However, no extra pin is required for the self-test output since the same pin is used for normal and BIST operation.

The die size available to us allowed us to implement three identical micromechanical sensors. The same self-test control circuitry, consisting of two switches (SW1 and SW2 in Figure 5), was used to control all three sensors simultaneously. In other words, the self-test mode is activated for all the sensors in parallel. Since the same output pin is shared by the sense signals from the three sensors, another switch-based control block is used to ensure that only one sense signal is transferred to the output pin at any given time. The control block uses high-impedance circuitry to isolate the remaining two sensor output signals.

5 Conclusions

The differential self-test method described in this work is focussed on enhancing observation and therefore complements the existing built-in stimulus generation techniques found in industry and proposed in the literature. We have demonstrated the ability to detect the presence of three defect types that cause local asymmetry which are not detectable by typical specification-based tests that measure both resonant frequency and sensitivity. It has been established, in principle, that a test method using pairwise comparison of multiple outputs from corresponding regions of symmetric devices can substantially enhance detection of hard-to-detect defects. The tradeoff of such an approach is a modest increase in design complexity and device area for additional electronics.

Acknowledgements

We would like to thank Sitaraman Iyer for his MEMS simulation expertise and Jiangfeng Wu for his invaluable technical input on the accelerometer design. Also, we are grateful for the insightful feedback provided by the ITC reviewers.

References

[1] A. Kourepenis, J. Borenstein, J. Connelly, R. Elliott, P. Ward, and M. Weinberg, "Performance of MEMS in-

ertial sensors," *Position Location and Navigation Symposium*, pp. 1-8, April 1998.

[2] R. Lal, P. R. Apte, N. K. Bhat, G. Bose, S. Chandra, and D. K. Sharma, "MEMS technology for biomedical applications," *MEMS: technology, design, CAD and applications*, pp. 24-25, Jan. 2002.

[3] S. Cass, "MEMS in space," *IEEE Spectrum*, Vol. 38, Issue 7, pp. 56-61, July 2001.

[4] D. C. Hutchison, K. Ohara, and A. Takeda, "Application of second generation advanced multimedia display processor (AMDP2) in a digital micro-mirror array based HDTV," *International Conference on Consumer Electronics (ICCE)*, pp. 294-295, June 2001.

[5] R. S. Payne, S. Sherman, S. Lewis, and R. T. Howe, "Surface Micromachining: From Vision to Reality to Vision (accelerometer)," *Proc. of International Solid State Circuits Conference*, pp. 164-165, Feb. 1995.

[6] R. Oboe, "Use of MEMS based accelerometers in hard disk drives," *Proc. of International Conference on Advanced Intelligent Mechatronics*, Vol. 2, pp. 1142 - 1147, 2001.

[7] A. Hartzell and D. Woodilla, "Reliability Methodology for Prediction of Micromachined Accelerometer Stiction," *Proc. of Reliability Physics Symposium*, pp. 202-205, March 1999.

[8] N. Deb and R. D. (Shawn) Blanton, "Analysis of Failure Sources in Surface-Micromachined MEMS," *Proc. International Test Conference*, pp. 739-749, Oct. 2000.

[9] D. De Bruyker, A. Cozma, and R. Puers, "A Combined Piezoresistive/Capacitive Pressure Sensor with Self-test Function based on Thermal Actuation," *Proc. Solid State Sensors and Actuators*, Vol. 2, pp. 1461 - 1464, 1997.

[10] H.V. Allen, S.C. Terry, and D.W. de Bruin, "Self-Testable Accelerometer Systems," *Proc. Micro Electro Mechanical Systems*, pp. 113-115, 1989.

[11] B. Charlot, S. Mir, F. Parrain, and B. Courtois, "Electrically Induced Stimuli for MEMS Self-Test," *Proc. VLSI Test Symposium*, pp. 210-215, Apr.-May 2001.

[12] R. Rosing, A. Lechner, A. Richardson, and A. Dorey, "Fault Simulation and Modelling of Microelectromechanical Systems," *Computing and Control Engineering Journal*, Vol. 11, Issue 5, pp. 242-250, Oct. 2000.

[13] A. Kolpekwar, R. D. Blanton, and D. Woodilla, "Failure Modes for Stiction in Surface-Micromachined MEMS," *Proc. of International Test Conference*, pp. 551-556, Oct. 1998.

[14] T. Jiang and R. D. Blanton, "Particulate Failures for Surface-Micromachined MEMS," *Proc. of International Test Conference*, pp. 329-337, Sept. 1999.

[15] H. Luo, G. K. Fedder, and L. R. Carley, "A 1 mG Lateral CMOS-MEMS Accelerometer," *Proc. of Micro Electro Mechanical Systems*, pp. 502-507, Jan. 2000.

[16] W. C. Tang, T.-C. H. Nguyen, M. W. Judy, and R. T. Howe, "Electrostatic Comb Drive of Lateral Polysilicon Resonators," *Sensors and Actuators A*, Vol. 21, Nos. 1-3, pp. 328-331, Feb. 1990.

[17] J. Xuesong, J. I. Seeger, M. Kraft, and B. E. Boser, "A Monolithic Surface Micromachined Z-axis Gyroscope with Digital Output," *Symposium on VLSI Circuits*, pp. 16-19, 2000.

[18] N. Deb and R. D. Blanton, "High-Level Fault Modeling in Surface-Micromachined MEMS," *Proc. of Design, Test, Integration, and Packaging of MEMS/MOEMS*, pp. 228-235, May 2000.

[19] J. Wu, G. K. Fedder, and L. R. Carley, "A Low-Noise Low-Offset Chopper-Stabilized Capacitive-readout Amplifier for CMOS MEMS Accelerometers," *Proc. of International Solid State Circuits Conference*, pp. 428-429, Feb. 2002.

[20] O. Tabata, K. Terasoma, N. Agawa, and K. Yamamoto, "Moving Mask LIGA (M/sup 2/LIGA) Process for Control of Side Wall Inclination," *Proc. of Micro Electro Mechanical Systems Conference*, pp. 252-256, Jan. 1999.

[21] S. V. Iyer, H. Lakdawala, G. K. Fedder, and T. Mukherjee, "Macromodeling Temperature-Dependent Curl in CMOS Micromachined Beams," *Proc. of Modeling and Simulation of Microsystems Conference*, pp. 88-91, March 2001.

[22] Q. Jing, H. Luo, T. Mukherjee, L. R. Carley, and G. K. Fedder, "CMOS Micromechanical Bandpass Filter Design Using a Hierarchical MEMS Circuit Library," *Proc. of Micro Electro Mechanical Systems Conference*, pp. 187-192, Jan. 2000.

[23] D. A. Koester, R. Mahadevan, and K. W. Markus, *MUMPS Introduction and Design Rules*, MCNC MEMS Technology Applications Center, 3021 Cornwallis Road, Research Triangle Park, NC, Oct. 1994.